Behavior of short-headed stud connectors in orthotropic steel-UHPC composite bridge deck under fatigue loading

Shi, Zhanchong; Su, Qingtian; Kavoura, Florentia; Veljkovic, Milan

DOI
10.1016/j.ijfatigue.2022.106845

Publication date
2022

Document Version
Final published version

Published in
International Journal of Fatigue

International Journal of Fatigue 160 (2022) 106845

Contents lists available at ScienceDirect

International Journal of Fatigue

journal homepage: www.elsevier.com/locate/ijfatigue

Behavior of short-headed stud connectors in orthotropic steel-UHPC composite bridge deck under fatigue loading

Zhanchong Shi [a,b], Qingtian Su [a,c,*], Florentia Kavoura [b], Milan Veljkovic [b]

[a] Department of Bridge Engineering, Tongji University, Shanghai 200092, China
[b] Department of Engineering Structure, Delft University of Technology, 2628CN Delft, The Netherlands
[c] Shanghai Engineering Research Center of High Performance Composite Bridges, Shanghai 200092, China

ARTICLE INFO

Keywords:
Short-headed stud connectors
The beam test
Run-outs
S-N curve
The maximum likelihood estimation (MLE) approach

ABSTRACT

The short-headed stud connectors play a critical role on the interaction of the orthotropic steel deck (OSD) and the ultra-high performance concrete (UHPC) layer in orthotropic steel-UHPC composite bridge deck. In this paper, the fatigue behavior of these short-headed stud connectors was experimentally investigated in a beam test. The failure modes of the short-headed stud connectors were identified and classified into 5 types. The fatigue test results were analyzed by linear regression analysis neglecting run-outs and treating run-outs as failure respectively. On the other hand, the maximum likelihood estimation (MLE) approach was used to shape the S-N curve by considering the influence of run-outs. Additionally, the push-out and beam fatigue test data were compared, and the push-out test presented a relatively conservative result. Last, the applicability of existing specifications on design guidelines regarding the short-headed stud connectors design in orthotropic steel–UHPC composite bridge deck is discussed, and a design S-N curve with 95% survival probability is proposed.

1. Introduction

The conventional orthotropic steel bridge decks (OSD) [see Fig. 1(a)] consisting of a steel deck plate stiffened by U-ribs and supported by crossbeams, are widely used in long-span bridges. Their main advantages are the lower self-weight, higher strength and more convenient installation when compared with concrete bridge decks. In common practice, the OSD is usually covered with a thin thickness layer of asphalt pavement. However, serious fatigue cracks of OSD under ever-increasing traffic volumes and higher wheel loads have posed a challenge to the application of this deck system [1]. In order to address this issue, ultra-high performance concrete (UHPC), which is a type of fiber reinforced cementitious composites with exceptional mechanical properties and durability [2], has been applied as topping layer of the OSD to improve the deck stiffness [1,3–5]. Dieng et al. [5] revealed that the stronger the composite action between the OSD and the UHPC layer is, the lower the stresses in the two components are. The densely distributed short-headed stud connectors welded on the steel deck plate are considered as an excellent connection to guarantee a robust composite action between the OSD and UHPC layer [7]. Therefore, the short-headed stud connectors play a critical role to make the UHPC layer assist the OSD to bear vehicle wheel loads. For this reason, the investigation of the mechanical properties of the stud connectors embedded in UHPC on the orthotropic steel-UHPC composite deck [see Fig. 1(b)], has attracted the researcher's attention the last 10 years.

The current investigations on stud connectors embedded in UHPC mainly focused on the static behavior, including the ultimate shear strength, slip capacity and shear stiffness, through push-out test and finite element analysis [8–11]. The short-headed stud connectors of composite bridge deck is more sensitive to the repeated vehicle wheel loads in the actual operation of bridge. Hence, it is the fatigue strength that governs the design of short-headed stud connectors in composite deck. However, studies investigating the fatigue behavior of short-headed stud connectors in composite deck are relatively limited [7,12]. According to Cao et al. [7], the fatigue failure modes of short-headed stud connectors embedded in UHPC layer observed in the push-out test were similar to that of stud connectors embedded in normal concrete (NC) slab, and the derived *S-N* curve with 95% survival probability lied slightly above the curve provided in Eurocode 4 [13].

In current fatigue-design practice of short-headed stud connectors used in orthotropic steel-UHPC composite deck, the design criterion is basically referred to existing specifications [13–15] and investigations [16–22] on stud connectors employed in traditional steel-normal concrete (NC) composite beams. The relevant investigations were conducted within two scopes: (1) the concrete is primarily normal concrete

* Corresponding author at: 1239 Siping Road, Tongji University, Shanghai 200092, China.
E-mail address: sqt@tongji.edu.cn (Q. Su).

https://doi.org/10.1016/j.ijfatigue.2022.106845
Received 25 November 2021; Received in revised form 4 February 2022; Accepted 5 March 2022
Available online 18 March 2022

Nomenclature

UHPC	ultra-high performance concrete
OSD	orthotropic steel decks
MLE	maximum likelihood estimation
HAZ	heat-affected zone
PDF	probability density function
CDF	cumulative density function
t	thickness of steel plate
D	diameter of stud connector or rebar
E_c	modulus of elasticity of UHPC
f_{cu}	cubic compress strength of UHPC
f_{ct}	tensile strength of UHPC
$f_{cr,fl}$	first cracking strength under flexural tensile
$f_{ct,fl}$	flexural strength
ΔP	load range
$P_{\max}$	maximum load
$P_{\min}$	minimum load
N_i	number of cycles
N_f	fatigue life
$\Delta\tau$	nominal shear stress range
$\Delta\tau_e$	equivalent constant amplitude nominal shear stress range
$\Delta\tau_{e2}$	fatigue shear strength at 2 million cycles
$\Delta\tau_i$	shear stress range related to each loading phases
$\Delta\sigma$	nominal tensile stress range
ΔV	shear force range of shear span
I_0	moment of inertia of the composite section
S_0	area moment of concrete section to the center of gravity axis of composite section
$L(x)$	length of shear span
A_{sd}	cross-section area of a single stud shank
n_1	number of stud rows (in transverse direction)
n_2	number of stud columns (in longitudinal direction)
m	material constant of *S-N* curve
C	constant of *S-N* curve
μ_c	mean value of C
σ_c	standard deviation of C
k	characteristic value
n	number of fatigue test sample size
P_s	survival probability
β	index related to survival probability
f	probability density function
F	cumulative density function
Φ	CDF of standard normal distribution
n_f	total number of the failed fatigue data points
n_r	total number of the run-out fatigue data points
L	joint failure probability or likelihood

or light-weight concrete with compressive strength and modulus of elasticity less than 60 MPa and 40GPa, respectively; (2) the stud connector with ratio of height to diameter larger than 4. By contrast, UHPC usually has a compressive strength and modulus of elasticity higher than 100 MPa and 40GPa [2], respectively. In parallel, the thickness of UHPC layer used in composite deck usually is 35–60 mm [7] and this consequently leads to the ratio of height to diameter of stud connectors less than 4. The changes in both mechanical and geometric properties make it necessary to discuss the applicability of existing specifications when applied to design of short-headed stud connectors in composite decks. Besides, current studies on the fatigue behavior of short-headed stud connectors embedded in UHPC layer are mainly based on push-out test. However, the beam test can better reflect the actual force state of the short-headed stud connectors in the composite deck system.

In addition, fatigue test results are composed of the failed and the run-out specimens. The run-out, i.e. the specimens with values of endurances reached without failure, are usually neglected to obtain the *S-N* curve through regression analysis. However, studies recommend that the *S-N* curve should be shaped by considering run-outs because run-outs simply indicate the absence of failure [20]. The maximum likelihood estimation (MLE) approach is considered to be effective to make a combined evaluation of the failed and the run-out specimens [23,24], and has been applied to shape the *S-N* curves of some fatigue-prone details in literature [25–27].

Based on the above considerations, the objective of this study is to characterize the fatigue behavior of the short-headed stud connectors in orthotropic steel-UHPC composite bridge deck through a beam test. The related fatigue failure modes are identified and the underlying mechanism is revealed. The MLE approach is used to shape the shear *S-N* curve of the short-headed stud connectors by considering the run-outs in existing beam tests. The fatigue test results from the push-out test and the beam test are compared, and the obtained *S-N* curves are compared with the ones presented in existing design codes. Finally, the design *S-N* curves for the short-headed stud connectors which could be used on composite deck designs are proposed.

2. Experimental description

2.1. Specimen design

A three-span continuous composite steel box girder bridge (with span

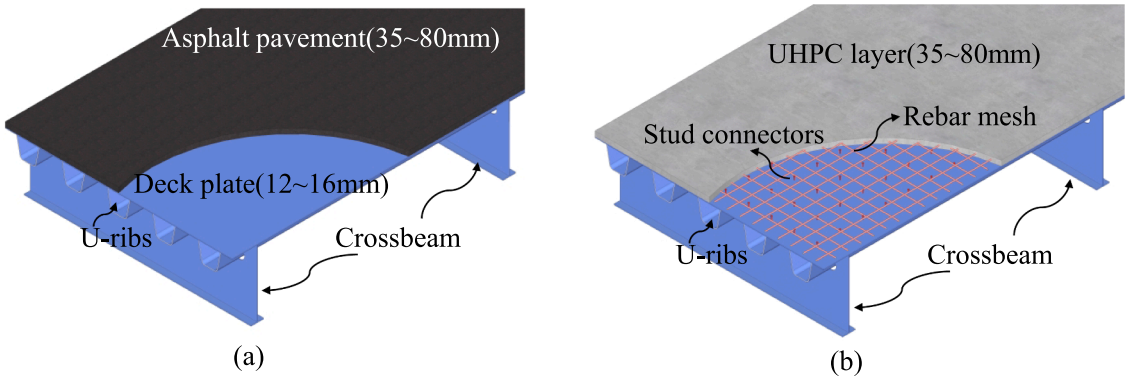

Fig. 1. Two deck systems: (a) the conventional OSD; (b) the OSD-UHPC composite deck.

layout of 154 + 245 + 154 m), which is located in Jinan, China, served as the prototype bridge of the specimen. The mid-span cross-section of the bridge is shown in Fig. 2. As depicted, the bridge is used as a highway and light-railway bridge. To alleviate the fatigue cracks of OSD under vehicle loading, a UHPC layer with thickness of 80 mm is casted on the OSD within the vehicle lanes. The UHPC layer is connected to the steel deck plate using densely distributed short-headed stud connectors, thus the deck system is treated as orthotropic steel-UHPC composite deck. Finally, the steel deck plate of the OSD is strengthened by longitudinal U-ribs at spacing of 720 mm and crossbeams at spacing of 4000 mm.

Based on the prototype bridge, a full-scale orthotropic steel-UHPC composite deck was designed to investigate the fatigue behavior of the deck system and is shown in Fig. 3. The length, width and height of the specimen was 8800 mm, 1440 mm and 392 mm, respectively [see Fig. 3 (b)]. The steel deck plate had thickness of 12 mm and was stiffened by two U-ribs with top width of 360 mm, bottom width of 240 mm, height of 300 mm and thickness of 8 mm [see Fig. 3(c)]. The U-ribs were connected by two connection types, namely butt welds (U_w) and high-strength bolts (U_b) at the location of 1000 mm to middle crossbeam in longitudinal direction. The height and thickness of the crossbeam web was 450 mm and 12 mm, and the width and thickness of crossbeam flange was 200 mm and 16 mm. The UHPC layer was reinforced with φ16mm rebar mesh at spacing of 200 mm both in longitudinal and transverse directions. The short-headed stud connectors had diameter of 13 mm and height of 45 mm (see Fig. 4). Besides, the arrangement of the short-headed stud connectors is shown in Fig. 3(b). The numbers of the short-headed stud connectors in transverse and longitudinal direction were named as stud rows and columns, respectively. The corresponding stud rows and stud columns were 5 and 11 respectively in each span.

2.2. Material properties

According to design of the prototype bridge, Q345q [28], ML15 [29] and HRB400 [30] were used for OSD, stud connectors and rebar in the full-scale specimen, respectively. Based on the tensile test [31], the modulus of elasticity, yield strength and ultimate strength of steel are summarized in Table 1.

The UHPC used in this study was a commercial material provided by Hefei Special Material Technology Co., Ltd. The UHPC contains 1173 kg/m^3 reactive powder, 616 kg/m^3 river sand with maximum aggregate size less than 4 mm, 472 kg/m^3 basalt aggregate with maximum aggregate size less than 8 mm, 25.7 kg/m^3 superplasticizer, 138 kg/m^3 water and 198 kg/m^3 hybrid steel fibers. The hybrid steel fibers are composed of hook-end fibers with length of 20 mm and diameter of 0.25 mm, and straight fibers with length of 13 mm and diameter of 0.2 mm. The mechanical properties of the UHPC under the same curing condition used for the composite deck specimen are summarized in Table 2. The information provided in Table 2 is mean value of three identical specimens which were tested according to the following provisions. Specifically, the tensile test of UHPC referred to Swiss recommendation [32]. And modulus of elasticity, cubic compress strength, first cracking strength under flexural tensile and flexural strength of UHPC were obtained experimentally based on the Chinses standard test methods for fiber reinforced concrete [33].

2.3. Test setup and loading protocol

The fatigue test was conducted in structural lab of Tongji University in Shanghai, China. The test setup is shown in Fig. 3(a) and Fig. 5. The specimen was placed and fixed on three steel support pedestals, and the support pedestals were attached to the ground using high-strength cement mortars. As shown in Fig. 3(a), the span from east-end crossbeam to middle crossbeam was named as load span, while the span from middle crossbeam to west-end crossbeam was named as no-load span. The actuators were placed at the mid-span section of the load span, and the cyclic load was applied through a loading beam. In order to simulate the effect of vehicle wheel load, a 20 mm thick rubber with size 200 mm by 720 mm was placed between the UHPC topping surface and the loading beam. Besides, in order to prevent vibration of the specimen under cyclic loading, two hydraulic jacks were applied to the topping surface of the deck at the position of west-end crossbeam [see Fig. 3(a)].

According to the design philosophy of the prototype bridge, the nominal tensile stress range of the UHPC layer under vehicle wheel load was within 2.9 MPa. So the design loading protocol of the specimen is based on the tensile stress range of the topping surface of the UHPC layer at the middle crossbeam. The loading protocol is described in Table 3. As shown, the specimen was loaded at constant load range ($\Delta P = P_{max}$-P_{min}, P_{max}, P_{min} denotes the maximum and minimum load) in each phase. Phase I was designed to evaluate the fatigue behavior of the composite deck in service life, and the rest phases were used to reveal the fatigue failure process of the specimen by increasing the load range. It should be noted that the maximum load of phase V and VI were no larger than phase IV because of malfunction of the fatigue machine occurred in phase IV. The loading frequency was kept at constant of 4 Hz during the whole cyclic loading phases.

It was difficult to detect the fatigue damage state of the short-headed stud connectors embedded in the UHPC layer directly. When the short-headed stud connectors were intact, there was no interface debonding between the steel deck plate and the UHPC layer; while when the short-headed stud connectors were fatigued and fractured, interface debonding occurred. Therefore, interface debonding was set as the fatigue failure criterion of the short-headed stud connectors at the corresponding interfaces. The interfaces corresponding to the adjacent short-

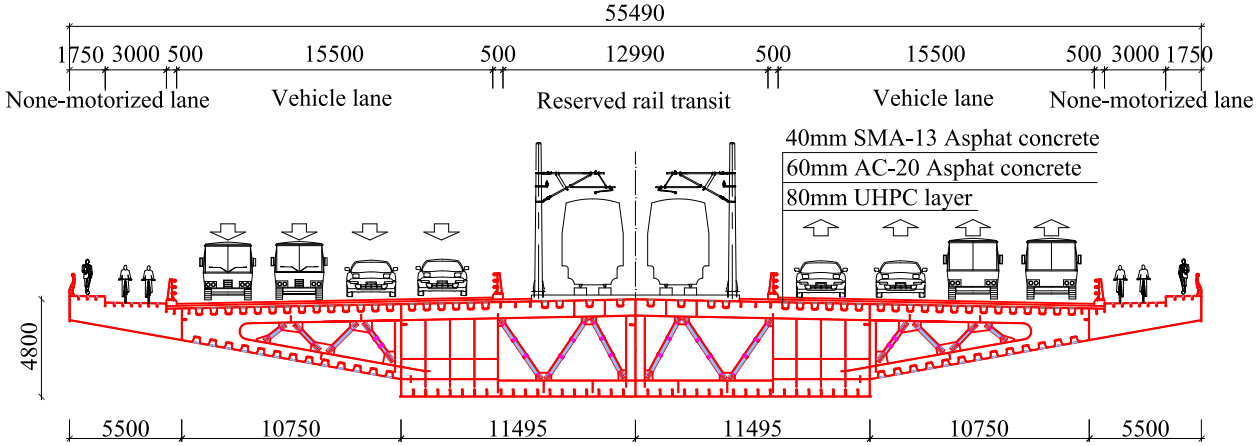

Fig. 2. Mid-span cross section of the prototype bridge (unit: mm).

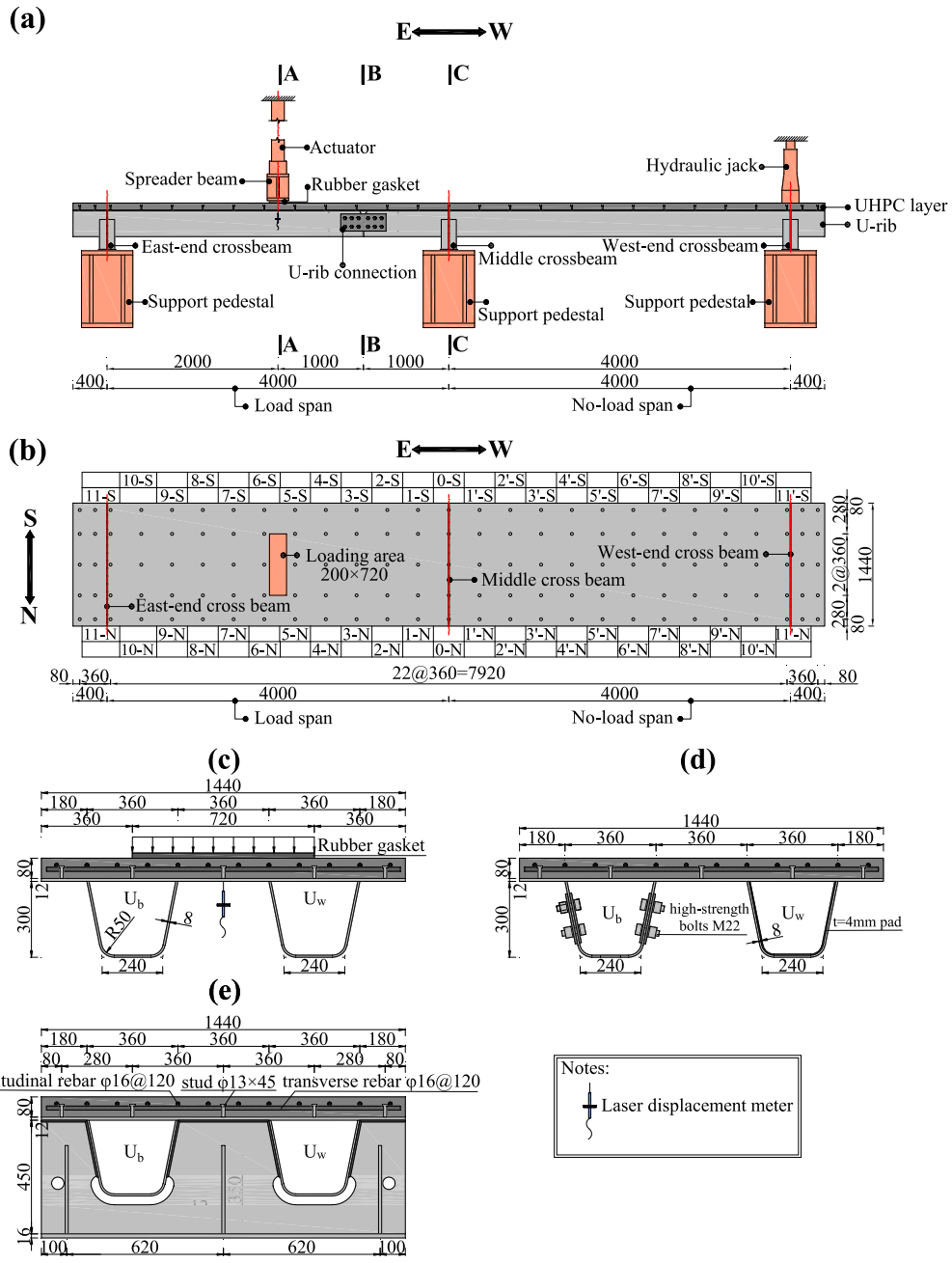

Fig. 3. Details of the full-scale specimen (unit: mm): (a) elevation view and setup; (b)arrangement of studs; (c)A-A cross section; (d)B-B cross section; (e)C-C cross section.

headed stud connectors were marked with numbers as shown in Fig. 3 (b) and Fig. 6. Take the mark "2-N" as an example, it denotes the interface located in the second stud column at the north side of the specimen.

3. Test results and analysis

3.1. Fatigue life

During loading phase I($\Sigma N_i = 0 \sim 2$ million) and phase II ($\Sigma N_i = 2 \sim 3$ million),there was no visible debonding at the marked interfaces. From this, it could be concluded that there were no fatigue fracture occurring at the short-headed stud connectors in these phases. The first visible debonding occurred at the 3-N interface when loading reached the 4.05 million cycles, as shown in Fig. 7. Then the consequent debonding developed at other marked interfaces reported in Table 4 along with their corresponding fatigue life N_f. As shown, the interface debonding only occurred at the load span where the two actuators were placed in its mid-span. As mentioned above, the fatigue fracture of the short-headed stud connectors could be determined by the interface debonding, the fatigue life of the short-headed stud connectors was considered identical to that of interface debonding accordingly.

3.2. Nominal shear stress range

To obtain the nominal shear stress range of the short-headed stud connectors, it was assumed that the shear force at interface was uniformly shared by all the short-headed stud connectors at the same shear span. Actually, shear stress redistribution occurs if some stud connectors are cyclically sheared to fracture, the remaining undamaged stud con-

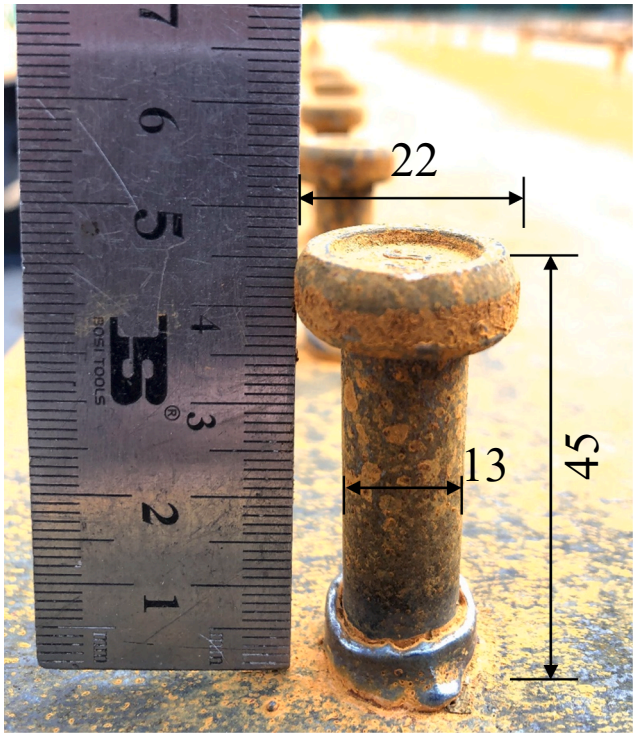

Fig. 4. Details of the short-headed stud connector (unit: mm).

Table 1
Mechanical properties of steel.

Material	t (mm)	D (mm)	Yield strength (MPa)	Ultimate strength (MPa)	Elastic modulus (GPa)
Q345q	8	—	411	554	210
	12	—	370	511	210
HRB400	—	16	549	664	200
ML15	—	13	332	479	206

Notes: t and D refer to thickness and diameter, respectively.

Table 2
Mechanical properties of UHPC.

E_c(GPa)	f_{cu}(MPa)	f_{ct} (MPa)	$f_{cr,fl}$(MPa)	$f_{ct,fl}$(MPa)
48	108	7.45	11.53	22.38

Notes: E_c, f_{cu}, f_{ct}, $f_{cr,fl}$, $f_{ct,fl}$ denote modulus of elasticity, cubic compressive strength, tensile strength, first cracking strength under flexural tensile and flexural strength, respectively.

nectors will withstand higher shear stress range. Based on the aforementioned assumption, the calculated nominal shear stress range will be more conservative. Considering the material properties and sectional characteristics, the nominal shear stress range of the short-headed stud connectors can be derived as:

$$\Delta\tau = \frac{\Delta V S_0 L(x)}{I_0 n_1 n_2 A_{sd}} \tag{1}$$

where ΔV is shear force range of shear span; I_0 is the moment of inertia of the composite section; S_0 is the area moment of concrete section (converted into steel area) to the center of gravity axis of composite section; $L(x)$ is the length of shear span; A_{sd} is the cross-section area of a single stud shank; n_1 is the number of stud rows (in transverse direction); n_2 is the number of stud columns (in longitudinal direction). In this fatigue test, for the shear span from east-end crossbeam

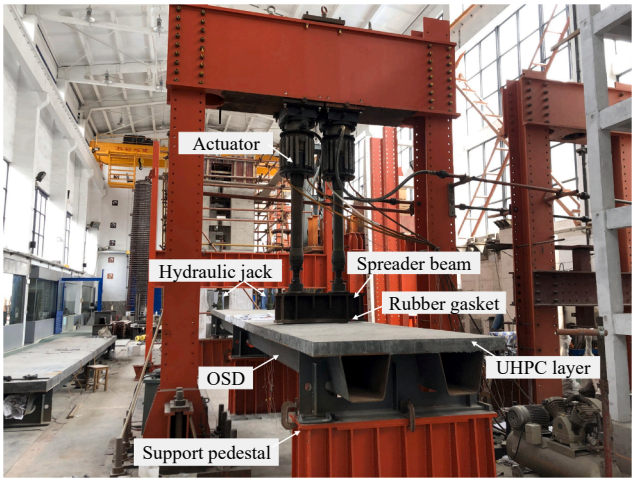

Fig. 5. Test setup.

Table 3
Fatigue loading protocol.

Phase	Load level P_{min} ~ P_{max}(kN)	Load range ΔP (kN)	Cycle Numbers N_i ($\times 10^4$)	Loading frequency (Hz)
I	271 ~ 405	134	200	4
II	310 ~ 539	229	100	4
III	560 ~ 807	247	160	4
IV	798 ~ 1075	277	40	4
V	421 ~ 730	309	50	4
VI	505 ~ 730	225	100	4

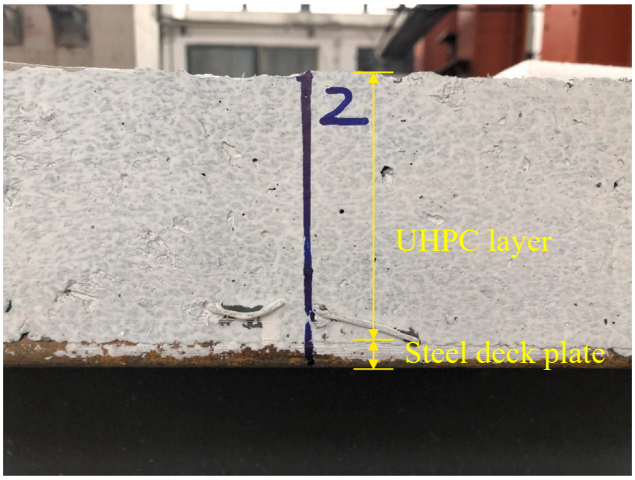

Fig. 6. The marked interface.

to the actuator, ΔV, $L(x)$, n_1 and n_2 are $13\Delta P/32$, 2000 mm, 6 and 5, respectively; for the shear span from actuator to middle crossbeam, ΔV, $L(x)$, n_1 and n_2 are $19\Delta P/32$, 2000 mm, 6 and 5, respectively; ΔP is load range summarized in Table 3. The calculated nominal shear stress ranges corresponding to loading phases are listed in Table 5.

The short-headed stud connectors were subjected to variable-amplitude fatigue load during the loading phases. Based on the concept of linear damage cumulative theory [34], the equivalent constant amplitude shear stress range related to fatigue life can be calculated by Eq.(2).

$$\Delta\tau_e = \left[\frac{\sum N_i(\Delta\tau_i)^m}{N_f}\right]^{1/m} \tag{2}$$

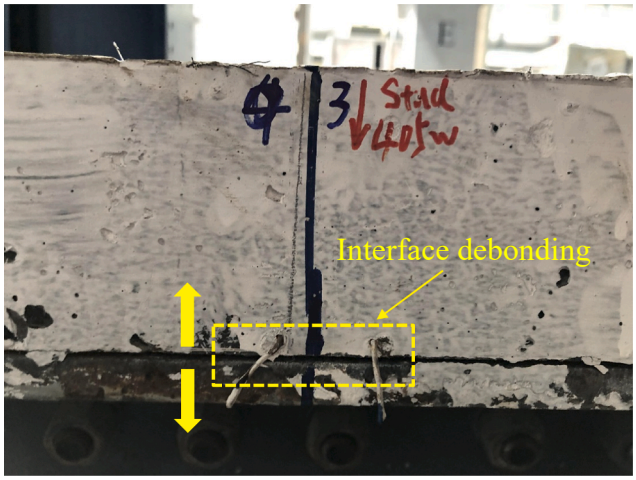

Fig. 7. Interface debonding at 3-N.

Table4
Debonding location and corresponding fatigue life N_f.

Interface location	N_f ($\times 10^4$)	Interface location	N_f ($\times 10^4$)
3-N	405	4-S	498
2-S	414	5-N	539
2-N	420	10-S	525
1-N	429	8-N	539
1-S	429	8-S	539
3-S	429	9-N	539
0-N	481	9-S	539
0-S	491	10-N	549

Table 5
Nominal shear stress range of stud connectors.

Phase	Δτ (MPa)	
	Shear span-I*	Shear span-II*
I	78	114
II	134	196
III	144	211
IV	162	237
V	181	264
VI	131	192

*Note: shear span-I is the shear span from east-end crossbeam to actuator, shear span-II is the shear span from actuator to middle crossbeam.

where $\Delta\tau_e$ is the equivalent constant amplitude nominal shear stress range; N_f is the fatigue life ; $\Delta\tau_i$ is shear stress range related to each loading phases; N_i is number of cycles associated with shear stress range $\Delta\tau_i$; m is material constant ($m = 8$ according to Eurocode 4[13]). Table 6 summarizes the calculated equivalent constant amplitude shear stress range and the corresponding fatigue life of the short-headed stud connectors.

Table 6
Fatigue life and equivalent constant amplitude shear stress range of the short-headed stud connectors.

Number	N_f ($\times 10^4$)	$\Delta\tau_e$ (MPa)	Number	N_f ($\times 10^4$)	$\Delta\tau_e$ (MPa)
3-N	405	187.9	4-S	498	198.9
2-S	414	188.7	5-N	539	211.4
2-N	420	189.2	10-S	525	142.2
1-N	429	189.9	8-N	539	144.7
1-S	429	189.9	8-S	539	144.7
3-S	429	189.9	9-N	539	144.7
0-N	481	196.1	9-S	539	144.7
0-S	491	197.8	10-N	549	146.2

3.3. Fatigue failure modes

To identify the fatigue damage state of the short-headed stud connectors, the UHPC layer was removed with the aid of a high-pressure water jet. The fatigue failure occurred in load span only as plotted in Fig. 8. The fatigue failure modes of the short-headed stud connectors and the corresponding fatigue failure mechanism are plotted in Fig. 9 and Fig. 11, respectively. As shown, the fatigue cracks are located around the heat-affected zone (HAZ) of the stud-to-deck plate weld. The fatigue failure modes of the short-headed stud connectors could be classified into five types, modes a-d and the combined modes da, db and dc. For mode a, fatigue crack initiated at the edge of stud shank and developed through the stud shank. This failure mode is similar to those observed in the fatigue push-out test [17] as well as beam test [35]. For mode b, fatigue crack initiated at weld toe near stud shank and propagated through the stud shank. This failure mode could be found both in the fatigue push-out test [19] and beam test [35]. For mode c, fatigue crack usually initiated at weld foot near stud shank and headed through stud shank. This failure mode could be found both in the fatigue push-out test [19,21,36] and fatigue beam test [37–39]. For mode d, fatigue crack usually initiated at weld foot or weld toe and penetrated into steel deck plate and induced concave depression [22] or tearing-off of steel deck plate, and this failure mode could be detected in the fatigue push-out test [7,19–22,40] as well as fatigue beam test [35,38]. For the combined modes, fatigue cracks occurred both at steel deck plate and stud shank, and this failure mode also has been observed in the fatigue push-out test [19,21,22]. As plotted in Fig. 8, the combined failure modes mainly distributed in shear span from actuator to middle crossbeam within which the shear stress range was relatively larger. Besides, fatigue cracks also were captured on the topping surface of steel deck plate around the weld collar while no fatigue damage was observed on the stud connectors. The failure mode and corresponding distribution are shown in Fig. 10 and Fig. 8, and this mode mainly located in shear span from east-end crossbeam to actuator. Furthermore, it should be noted that failure mode a, mode b and mode d are the fracture of base material of short-headed stud connectors or steel deck plate, while mode c is the fatigue damage occurring in weld and base material of the short-headed stud connector.

The fatigue fracture size of the damaged short-headed stud connectors and the steel deck plate were measured as depicted in Fig. 12 and were recorded as plotted in Fig. 11 (d). As shown, the vertical distance from the upper fracture line of the stud shank to the topping surface of the steel deck plate is approximately 10 mm, and this distance also can be treated as the limit of HAZ in stud connectors presented herein. With regard to the fracture zone of the steel deck plate, the length and width of the tearing zone are about 35 mm and 13 mm, respectively. The largest depth of the tearing zone is around 8 mm, which is two thirds of the thickness of the steel deck plate. This also demonstrates that the failure mode d couldn't penetrate through the whole thickness of the steel deck plate according to the current design. As Wang et al. [35] discussed, mode d is induced by the relatively large ratio of the stud diameter to steel plate thickness, and should be avoided.

In addition, the debonding interfaces listed in Table 4 are generally accomplished with the fractured short-headed stud connectors in Fig. 8, indicating the feasibility of determining the fatigue life of the short-headed stud connectors by interface debonding.

4. Discussion on S-N curves

4.1. S-N curves based on IIW recommendation

The *S-N* curve is usually established by fitting the failed fatigue test data at various stress levels. To obtain the *S-N* curve of the short-headed stud connectors, the specimen details and fatigue test results obtained from existing studies [41–45]are summarized in Table 7 and Table 8, respectively. It should be noted that all these tests are fatigue beam tests

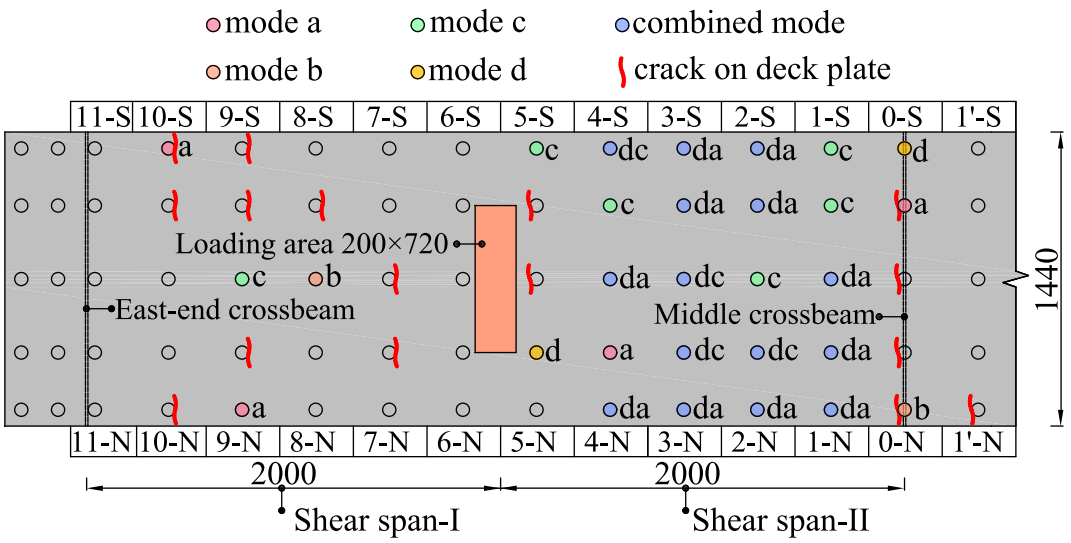

Fig. 8. Distribution of fatigue failure modes (unit: mm).

for orthotropic steel-UHPC composite bridge deck. The equivalent constant amplitude nominal shear stress range of the short-headed stud connectors at fatigue life N_f is obtained based on the aforementioned method in Eq.(2). For the run-out specimens in Table 8, the fatigue life N_f denotes the total number of cycles and is not the actual fatigue life under the related shear stress range.

The *S-N* curve in double logarithmic form is expressed in Eq.(3) [13,23].

$$logN = C - mlog\Delta\tau \tag{3}$$

where $\Delta\tau$ is shear stress range, N is fatigue life at shear stress range $\Delta\tau$, C is a constant, and m is the slope of the *S-N* curve. According to the recommendation of International institute of welding 2016 (IIW 2016) [23], the *S-N* curve of the short-headed stud connectors was established based the following steps on the basis of the failed fatigue data of this study and literature [41].

(a) Calculate $\log_{10}$ of all failed data:the equivalent constant amplitude nominal shear stress range $\Delta\tau_e$ and fatigue life N_f.
(b) Calculate exponents m and constant C (see Eq. (3)). The slope m can be obtained by linear fitting or taken the fixed value which is derived from other tests under comparable conditions. To be consistent with the Eurocode 4, m was taken as 8.
(c) Calculate mean value and standard deviation of C expressed in Eq.(4) and Eq.(5), respectively. Where n is sample size of fatigue data.

$$\mu_C = \frac{\sum C_i}{n} \tag{4}$$

$$\sigma_C = \sqrt{\frac{(\mu_C - C_i)^2}{n-1}} \tag{5}$$

(d) Calculate the characteristic value C_k in Eq.(6). The *S-N* curve used for design usually has a 95% survival probability at confidence level of 75%, the corresponding value k is calculated in Eq.(7). When k is taken as the opposite number, the *S-N* curve with a 5% survival probability also can be obtained.

$$C_k = \mu_C - k\sigma_C \tag{6}$$

$$k = 1.645 \cdot \left(1 + \frac{1}{\sqrt{n}}\right) \tag{7}$$

Substituting the failed fatigue test data, $\mu_c = 24.786$, $\sigma_c = 0.429$, and $k = 2.070$ were obtained. The standard deviation σ_c is just 1.73% of mean value μ_c , indicating that the data used has a small scatter. The *S-N* curves of the short-headed stud connectors with 5%, 50%, and 95% survival probability are listed in Eq.(8), Eq.(9) and Eq.(10), respectively.

$$logN = 25.675 - 8log\Delta\tau \tag{8}$$

$$logN = 24.786 - 8log\Delta\tau \tag{9}$$

$$logN = 23.897 - 8log\Delta\tau \tag{10}$$

The foregoing *S-N* curves were established by only considering the failed fatigue data and neglecting the run-out. For comparison, the *S-N* curves considering run-outs in Table 8 as failure were also established based on the above procedure. The corresponding $\mu_c = 24.307$, $\sigma_c = 1.122$, and $k = 2.013$ were obtained. The standard deviation σ_c is 4.62% of mean value μ_c , indicating that a relatively wider scatter than that obtained neglecting run-outs. Accordingly, the *S-N* curves considering run-outs as failure with 5%, 50%, and 95% survival probability are obtained in Eq.(11), Eq.(12) and Eq.(13), respectively.

$$logN = 26.566 - 8log\Delta\tau \tag{11}$$

$$logN = 24.307 - 8log\Delta\tau \tag{12}$$

$$logN = 22.049 - 8log\Delta\tau \tag{13}$$

The *S-N* curves of beam test neglecting run-outs and considering run-outs as failure are shown in Fig. 13.

As shown, the *S-N* curve considering run-outs as failure has a wider scatter compared with neglecting run-outs, which has been verified by the ratio of standard deviation to mean value. The fatigue strength with 95% survival probability at 2 million cycles of neglecting run-outs and considering run-outs as failure are 158 MPa and 93 MPa, respectively. This indicates that the method of considering run-outs as failure will considerably lower the fatigue strength at 2 million cycles up to 65 MPa.

4.2. *S-N curves based on the MLE considering run-outs*

The orthotropic steel-UHPC composite deck is a new structure and the related failed fatigue beam test results are limited, it is necessary to consider the run-out fatigue beam test results to establish the *S-N* curve. The MLE approach allows run-outs to influence the *S-N* curve through the cumulative density function (CDF). The objective of the MLE approach is to identify a probability distribution at each stress level that

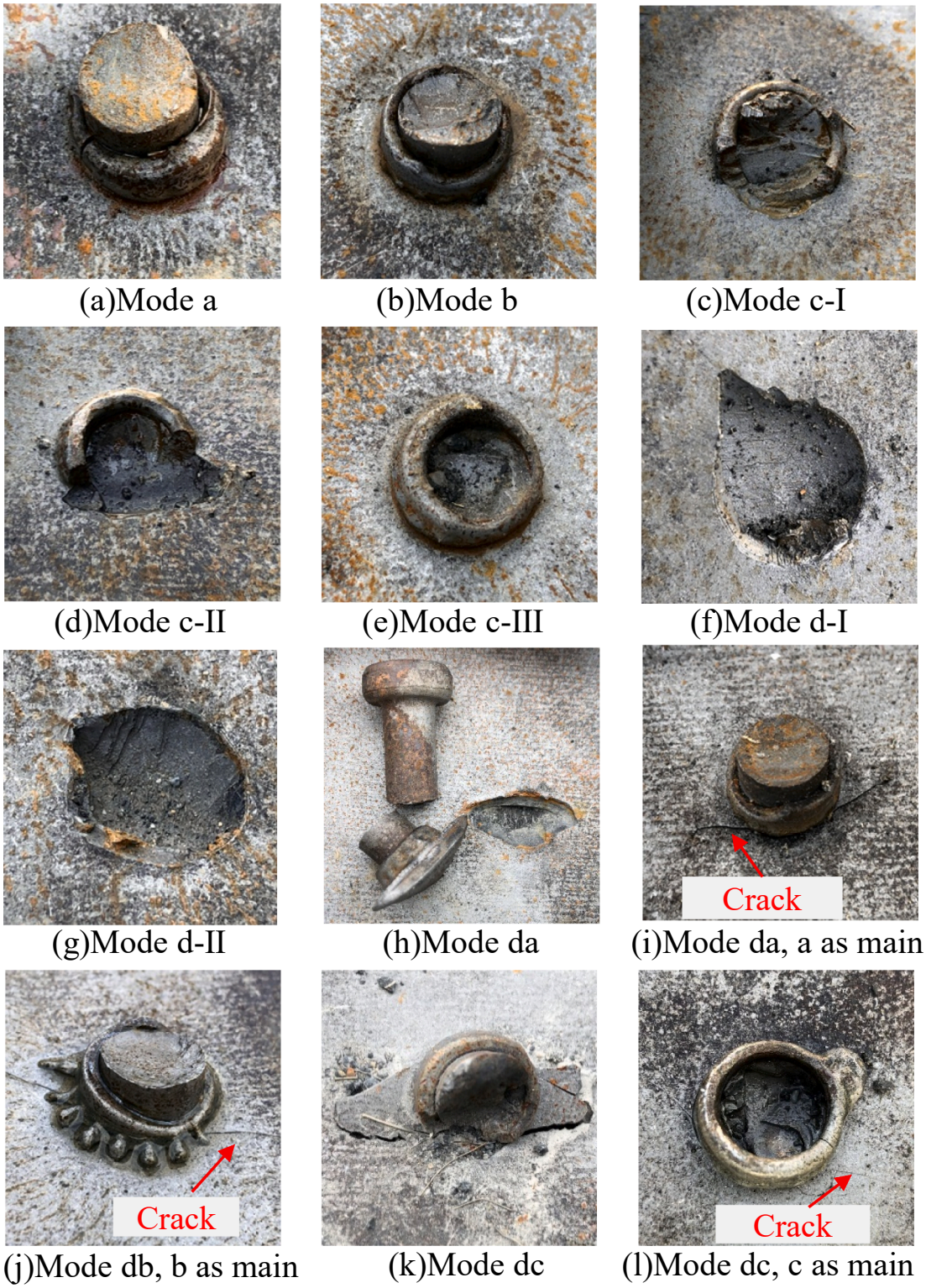

Fig. 9. Fatigue failure modes.

is most likely to generate the test data [20].

It is assumed that the logarithm of fatigue life at each stress level follows a normal distribution. The fatigue-life curve represented through the MLE fitting is plotted in Fig. 14. As shown, The probability density function (PDF) of logarithms of fatigue life log$N$ at stress level S is expressed in Eq.(14), the related cumulative density function (CDF) is given in Eq.(15), where Φ is CDF of standard normal distribution. Then log$N$ can be obtained by negating the Eq.(15), as shown in Eq.(16), where μ and σ are mean value and standard deviation of log$N$ respectively, β is a constant related to survival probability P_s as expressed in Eq.(17) and depicted in Fig. 15. To make Eq.(16) presents oblique line in the double logarithmic coordinate system, both μ and σ should show a linear relationship with log$S$. Consequently, μ and σ are assumed to be expressed in Eq.(18), where C, m and B are unknown parameters to be determined through the MLE approach. Substituting Eq.(18) into Eq. (16), the P-S-N curve is derived in Eq.(19), where P denotes survival

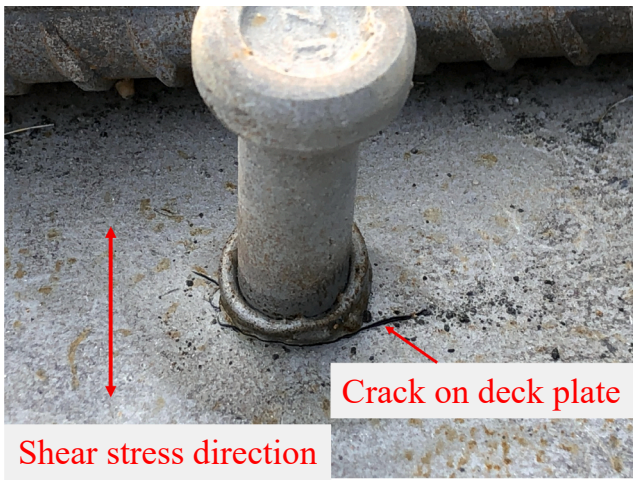

Fig. 10. Crack of steel deck plate around weld collar.

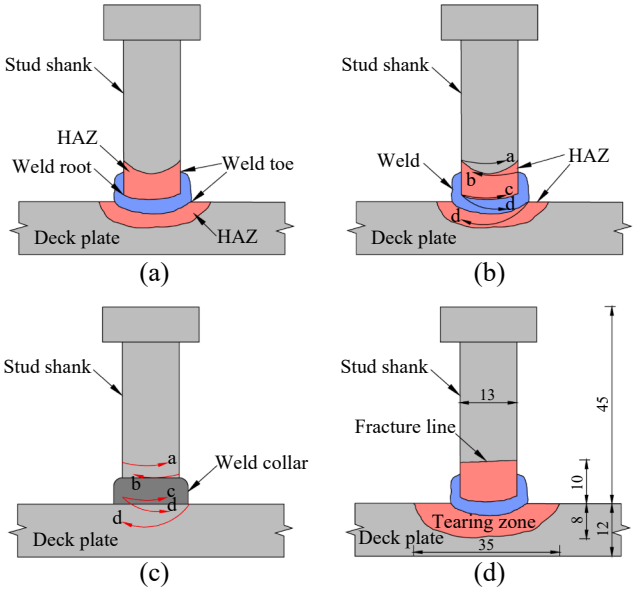

Fig. 11. Fatigue failure mechanism (unit: mm): (a) internal details of the stud-to-deck plate weld; (b)internal appearance of failure paths; (c) external appearance of failure paths; (d) fatigue fracture zone.

probability P_s which is in the form of β.

$$f(logN) = \frac{1}{\sqrt{2\pi}\sigma} e^{-\frac{(logN-\mu)^2}{2\sigma^2}} \; -\infty \leqslant logN \leqslant +\infty \tag{14}$$

$$F(logN) = \int_{-\infty}^{logN} \frac{1}{\sqrt{2\pi}\sigma} e^{-\frac{(t-\mu)^2}{2\sigma^2}} d_t = \Phi\left(\frac{logN-\mu}{\sigma}\right) \tag{15}$$

$$logN = \mu + \sigma\Phi^{-1}(F) = \mu + \sigma(-\beta) \tag{16}$$

$$\beta = -\Phi^{-1}(F) = \Phi^{-1}(P_s) \tag{17}$$

$$\begin{cases} \mu = C - mlogS \\ \sigma = B \end{cases} \tag{18}$$

$$logN = C - mlogS - \beta B \tag{19}$$

Based on the MLE approach, this joint failure probability (or likelihood) considering both the failed and the run-out test results is simply failure probability of every data point, and is given in Eq.(20) [20], where n_f is the total number of the failed fatigue data points, n_r is the

Table 7
Summary of specimen details in existing literature.

Literature	Thickness of UHPC layer (mm)	Elastic modulus of UHPC (GPa)	Thickness of steel deck plate (mm)	Size of stud (mm)
Chen [41]	50	45.0	16	13 × 40
Liu [42]	50	42.6	12	13 × 35
Yuan [43]	60	47.8	12	13 × 40
Feng [44]	50	44.4	16	13 × 40
Liu [45]	60	42.1	12	16 × 40

Table 8
Summary of fatigue beam test results in existing literature.

Literature	Specimen number	$N_f(\times 10^4)$	$\Delta\tau_e$(MPa)	Failure or Run-out
Chen[41]	VAF1	531	193.5	Failure
	VAF2	410	193.3	Failure
	CAF1	111	245.6	Failure
	CAF2	160	214.9	Failure
Liu [42]	Sagging	416	137.2	Run-out
	Hogging	250	176.7	Run-out
Yuan[43]	—	500	103.7	Run-out
Feng [44]	—	625	97.6	Run-out
Liu [45]	—	760	53.8	Run-out

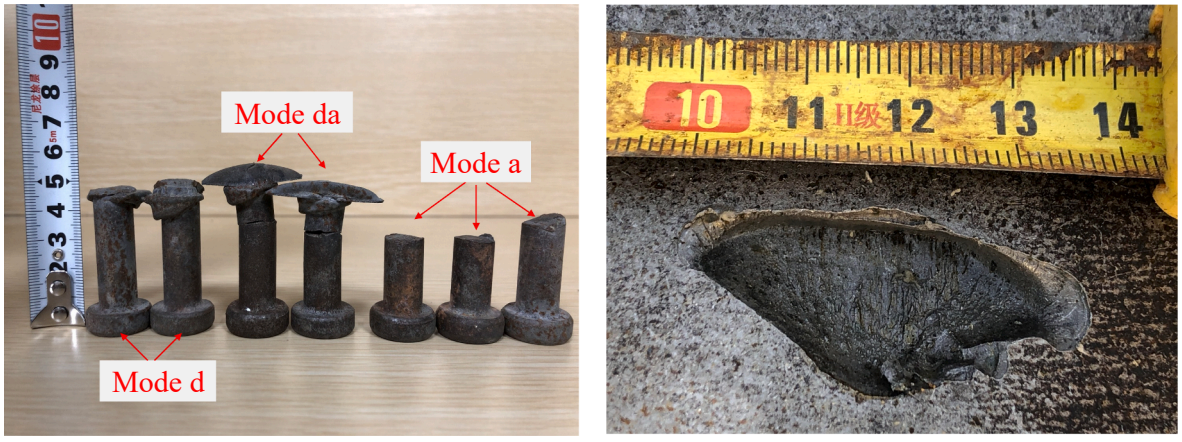

Fig. 12. Size of fatigue fracture zone (unit: mm): (a) the stud shank; (b) the steel deck plate.

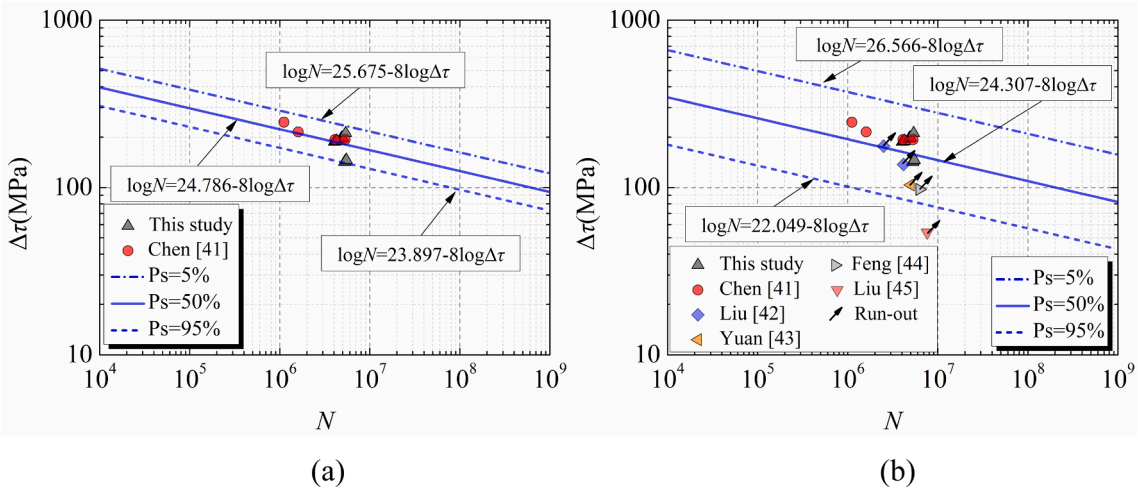

Fig. 13. *S-N* curves of the beam test based on IIW 2016 recommendation: (a) neglecting run-outs; (b) considering run-outs as failure..

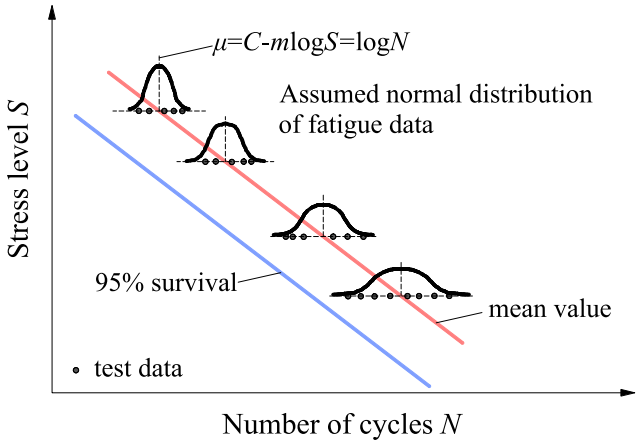

Fig. 14. Fatigue-life curve representation through the MLE fitting.

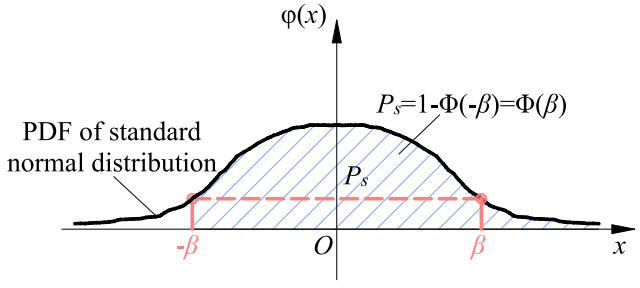

Fig. 15. The relation between β and P_s.

total number of the run-out fatigue data points. The likelihood expressed in Eq.(21) is derived by putting Eq.(18) into Eq.(20). Substituting all the fatigue data points in Table 6 and Table 8 into Eq.(21), and setting m equal to 8, $C = 24.793$ and $B = 0.4101$ were obtained by solving the partial derivative equations derived from Eq.(21). Accordingly, the *P-S-N* curve of the short-headed stud connectors based on the MLE approach is expressed in Eq.(22). The *S-N* curve with 50% survival probability is written in Eq.(23). Considering a 75% confidence level of 95% probability of survival, β can be calculated as k shown in Eq.(7) where the related n was taken the total number of the failed and the run-out fatigue data points, the corresponding *S-N* curve is obtained in Eq.(24). Correspondingly, Eq.(25) denotes the *S-N* curve with 5% survival probability.

$$L = \prod_{i=1}^{n_f}[f(logN_i)] \cdot \prod_{i=1}^{n_r}[1 - F(logN_i)] \tag{20}$$

$$L = \prod_{i=1}^{n_f}\frac{1}{\sqrt{2\pi}B}e^{-\frac{(logN_i - C + mlogS_i)^2}{2B^2}} \cdot \prod_{i=1}^{n_r}\left[1 - \int_{-\infty}^{logN_i}\frac{1}{\sqrt{2\pi}B}e^{-\frac{(t - C + mlogS_i)^2}{2B^2}}dt\right] \tag{21}$$

$$logN = 24.793 - 8log\Delta\tau - 0.4101\beta \tag{22}$$

$$logN = 24.793 - 8log\Delta\tau \tag{23}$$

$$logN = 23.967 - 8log\Delta\tau \tag{24}$$

$$logN = 25.618 - 8log\Delta\tau \tag{25}$$

The *S-N* curves of the short-headed stud connectors obtained through the MLE approach, and the comparison of *S-N* curves with 95% survival probability based on the three methods mentioned above are plotted in Fig. 16. As shown, the *S-N* curve with 50% survival probability based on the MLE approach lies above all the run-out data points and presents a narrow scatter with the upper and lower bound. The MLE *S-N* curve with 95% survival probability is close to that neglecting run-outs, and shows a little higher, indicating that the MLE approach can effectively feature the *S-N* curve through considering run-outs. The fatigue strength $\Delta\tau_{e2}$ at 2 million cycles by performing the MLE approach, neglecting run-outs and considering run-outs as failure are 162 MPa, 158 MPa and 93 MPa respectively, and this result shows the same trend with that of fatigue-prone details described in literature [24].

4.3. Comparison with the push-out test results

The shear fatigue push-out test of the short-headed stud connectors embedded in thin UHPC layer were reported in previous research [7,12]. The specimen details is shown in Fig. 17 and test results are summarized in Table 9. The *S-N* curves of the push-out test established through regression analysis are shown in Fig. 18(a). The comparison of *S-N* curves with 95% survival probability between the beam and the push-out test is plotted in Fig. 18(b). As shown, the failed data points of the beam test lie considerably above that of the push-out test. The fatigue strength $\Delta\tau_{e2}$ at 2 million cycles of the beam test (158 MPa) neglecting run-outs is significantly larger than that of the push-out test (103 MPa), and the amplitude is up to 55 MPa. Two reasons may account for this result. The adhesion between steel deck plate and UHPC layer within the whole deck area fails prior to fatigue fracture occurring at the short-headed stud connectors in the beam test. Secondly, shear stress redistribution does not occur and the loading on the stud connectors is

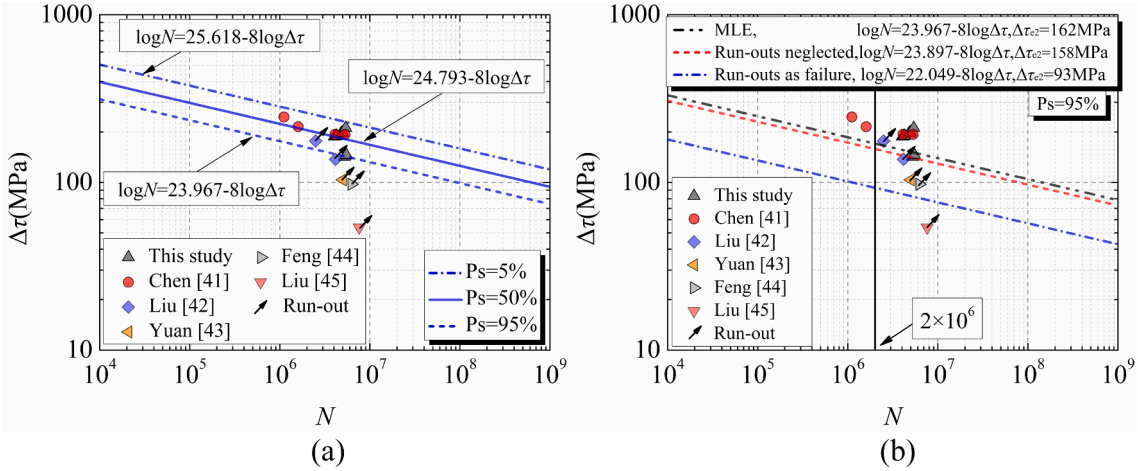

Fig. 16. *S-N* curves of the beam test: (a) based on the MLE approach; (b) comparison of three methods..

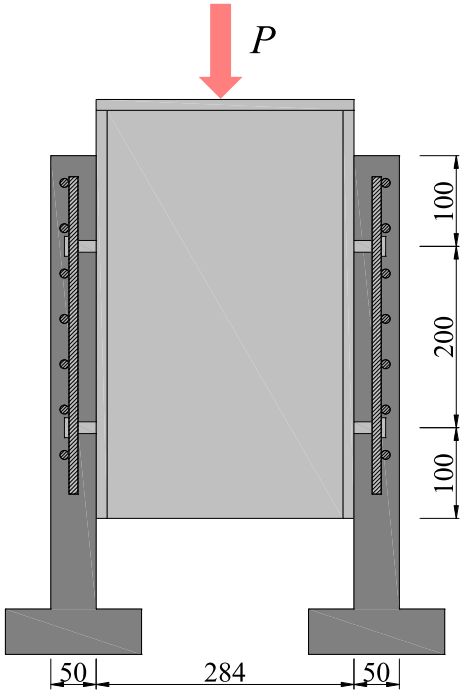

Fig. 17. Specimen details of the push-out test (unit: mm) [7].

Table 9
Summary of shear fatigue push-out test results.

Literature	Specimen number	$N_f(\times 10^4)$	Δτ(MPa)	Failure or Run-out
Zhang [12]	F-1	240.5	112	Failure
	F-3	60	145	
Cao [7]	FAT-1	1178.7	94	
	FAT-2	113	117	
	FAT-3	168.8	125	
	FAT-4	44.1	135	

maintained at a reasonably constant level throughout the cycle life in the push-out test [22].

In order to further investigate the test results difference between the beam test and the push-out test, the fatigue test results of stud connectors used in traditional steel-normal concrete (NC) composite beams were summarized. The corresponding test results of the beam and the push-out tests were reported in literature [16,18]. Based on regression analysis, the related *S-N* curves are plotted in Fig. 19. As shown, the failed data points of the beam test lie above that of the push-out test. The fatigue strength $\Delta\tau_{e2}$ at 2 million cycles with 95% survival probability of the beam test is 104 MPa, which is 28 MPa larger than its counterpart (76 MPa) of the push-out test.

It can be shown that the fatigue strength of the stud connectors in the beam test performs higher than in the push-out test no matter if the stud connectors are placed in an orthotropic steel-UHPC composite deck or in a traditional steel-NC composite beam. Besides, it should be noted that the failure criterion in the beam test can explain the reason that the different amplitude of the former (55 MPa) is almost twice of the latter (28 MPa). The fatigue failure criterion in orthotropic steel-UHPC composite deck was defined as the interface debonding, and that was taken indirectly from the steel flange strains in steel-NC composite beam. Interface debonding is usually accompanied with fatigue fracture of the stud connectors, while strain gauge reading changes indicate the initial crack of the stud connectors, thus the former exerts a relatively longer fatigue life. In parallel, the equivalent constant amplitude nominal shear stress range expressed in Eq.(2) will be larger accordingly.

4.4. Comparison with existing specifications

Eurocode 4 [13], AASHTO LRFD (2007) [14], TB10091-2017 [15] have recommended the *S-N* curves of stud connector in bridge design. A brief introduction of these specifications are listed as following.

Eurocode 4 [13]

In Eurocode 4 [13], the fatigue shear strength curve of an automatically welded stud connector with a normal weld collar in concrete with normal-weight aggregate is defined by Eq.(26). The corresponding fatigue strength at 2 million cycles of is 95 MPa.

$$logN = 22.123 - 8log\Delta\tau \tag{26}$$

AASHTO LRFD (2007) [14]

In AASHTO LRFD [14], the fatigue shear strength of an individual stud connector is taken as Eq.(27), in which α is expressed in Eq.(28). Fatigue strength of 66 MPa at 2 million cycles is consequently obtained.

$$\Delta\tau = 4\alpha/\pi = 303 - 37.56logN \tag{27}$$

$$\alpha = 238 - 29.5logN \geqslant 19.0 \tag{28}$$

TB 10091–2017 [15]

Both the fatigue shear strength curve and the fatigue tensile strength curve of stud connector are considered in TB 10091–2017 [15], the corresponding expression is given in Eq.(29) and Eq.(30), respectively. As shown, $\Delta\sigma$ denotes nominal tensile stress range of stud connector. Accordingly, the fatigue shear strength and fatigue tensile strength at 2

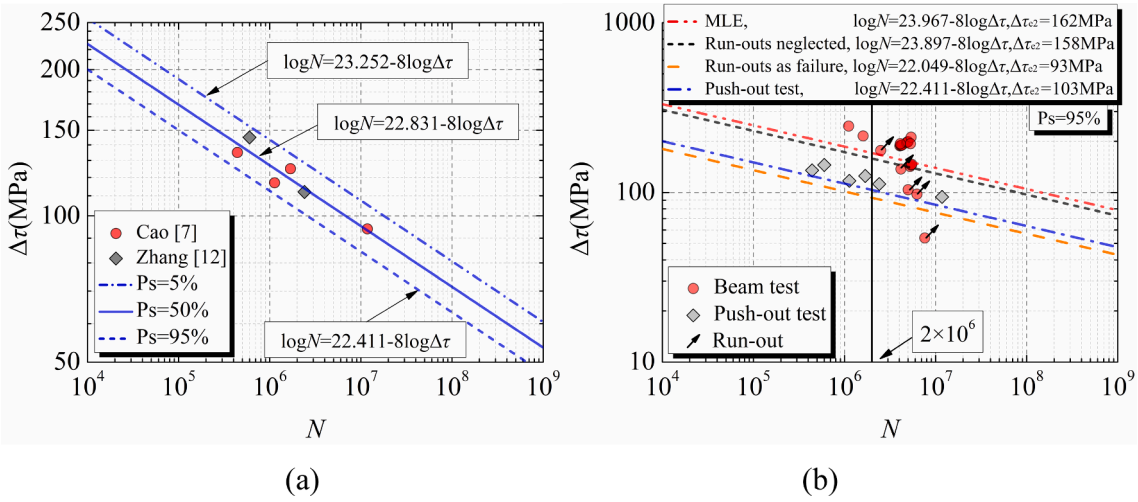

Fig. 18. *S-N* curves of the short-headed stud connectors in UHPC layer: (a) the push-out test; (b) comparison between the beam test and the push-out test.

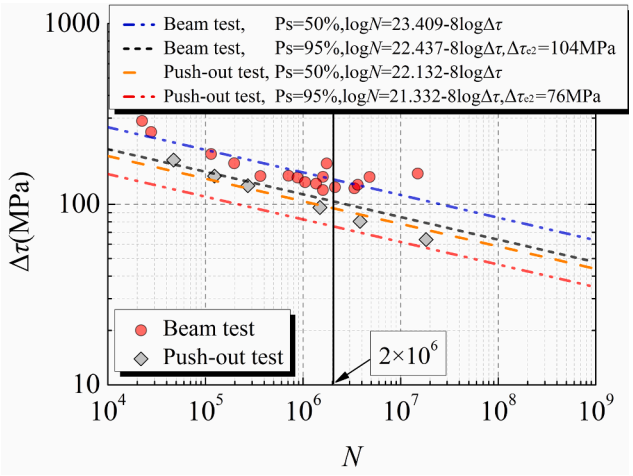

Fig. 19. *S-N* curves of the stud connectors in steel-NC composite beam.

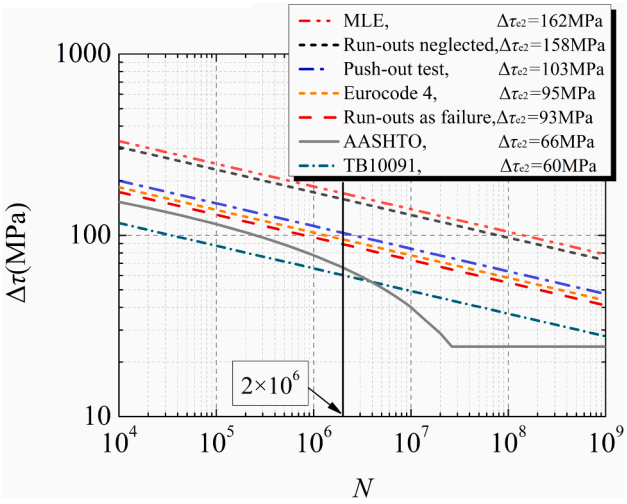

Fig. 20. *S-N* curves comparison with existing specifications.

million cycles are identical and equal to 60 MPa.

$$logN = 20.54 - 8log\Delta\tau \tag{29}$$

$$logN = 20.54 - 8log\Delta\sigma \tag{30}$$

The comparison of *S-N* curves obtained through the beam test using the aforementioned three methods (i.e. neglecting run-outs, considering run-outs as failure and the MLE approach), obtained through the push-out test and recommended in the above specifications is plotted in Fig. 20. As shown, AASHTO LRFD [14] and TB 10091–2017 [15] provide a considerably conservative basis for fatigue assessment of stud connectors in orthotropic steel–UHPC composite bridge deck. The *S-N* curves established through a beam test considering run-outs as failure is closest to that of Eurocode 4. By contrast, the curve obtained by the push-out test in steel-UHPC composite specimens lies apparently above the Eurocode 4 [13] curve which is established through push-out test of steel-NC composite specimens, the use of different kinds of concrete (UHPC and NC) may account for this phenomenon. The method of regression analysis neglecting runouts and the MLE approach considering runouts provide the relatively highest *S-N* curves.

It should be noted that the current *S-N* curves in specifications are obtained based on stud connectors with ratio of height to diameter larger than 4 embedded in NC slab, while the short-headed stud connectors used in orthotropic steel–UHPC composite bridge deck usually has a height to diameter smaller than 4. These differences in the concrete type as well as the stud size, make the fatigue strengths at 2 million cycles of the short-headed stud connectors in UHPC layer from the push-out test and the beam test (based on the MLE approach) larger than those in the current specifications. When the current specifications are adopted in design of the short-headed stud connectors in orthotropic steel–UHPC composite bridge deck, the difference between specifications

Table 10
Safety margin comparison (unit: MPa).

Push-out test	Eurocode 4		AASHTO 2007		TB10091-2017	
$\Delta\tau_{e2,pu}$	$\Delta\tau_{e2,eu}$	$\Delta\tau_{e2,pu}$-$\Delta\tau_{e2,eu}$	$\Delta\tau_{e2,aa}$	$\Delta\tau_{e2,pu}$-$\Delta\tau_{e2,aa}$	$\Delta\tau_{e2,tb}$	$\Delta\tau_{e2,pu}$-$\Delta\tau_{e2,tb}$
103	95	8	65	38	60	43
Beam test-MLE	Eurocode 4		AASHTO 2007		TB10091-2017	
$\Delta\tau_{e2,mle}$	$\Delta\tau_{e2,eu}$	$\Delta\tau_{e2,mle}$-$\Delta\tau_{e2,eu}$	$\Delta\tau_{e2,aa}$	$\Delta\tau_{e2,mle}$-$\Delta\tau_{e2,aa}$	$\Delta\tau_{e2,tb}$	$\Delta\tau_{e2,mle}$-$\Delta\tau_{e2,tb}$
162	95	67	65	97	60	102

Notes: $\Delta\tau_{e2,pu}$, $\Delta\tau_{e2,mle}$ denote the shear fatigue strength at 2 million cycles with 95% survival probability of the push-out test and the beam test based on the MLE approach; $\Delta\tau_{e2,eu}$, $\Delta\tau_{e2,aa}$, $\Delta\tau_{e2,tb}$ denote the shear fatigue strength at 2 million cycles of Eurocode 4, AASHTO 2007 and TB10091-2017, respectively.

and the push-out test result or the beam test result using the MLE approach could be considered as safety margin, as listed in Table 10. As shown, the safety margins of Eurocode 4, AASHTO LRFD (2007), TB10091-2017 are 8 MPa, 38 MPa, and 43 MPa respectively when compared with the push-out test result. While the counterparts are 67 MPa, 97 MPa, and 102 MPa respectively when compared with the beam test result using the MLE approach. The current specifications make a more conservative arrangement of the short-headed stud connectors in orthotropic steel–UHPC composite bridge deck when used in design. Therefore, the *S-N* curve with 95% survival probability obtained through the push-out test (i.e. $\log N = 22.411\text{-}8\log\Delta\tau$) and established by the MLE approach of the beam test (i.e. $\log N = 23.967\text{-}8\log\Delta\tau$), are recommended as a lower and an upper bound for fatigue design of the short-headed stud connectors in orthotropic steel–UHPC composite bridge deck.

5. Conclusions

Based on the above investigations, the main conclusions are:

1. The fatigue cracks of the short-headed stud connectors in the beam test located around the stud-to-deck plate weld heat-affected zone, and the failure modes can be classified into 5 modes. Failure mode a, mode b and mode d are the fracture of base material of short-headed stud connectors or steel deck plate, while mode c is the fatigue damage occurring in weld and base material of the short-headed stud connectors.
2. The *S-N* curve with 95% survival probability was established through regression analysis on the basis of this study and existing literature. Considering run-outs as failure can lower the fatigue strength at 2 million cycles up to 65 MPa compared to that of neglecting run-outs, e.g. from 158 MPa to 93 MPa.
3. The MLE approach allows the run-out to shape the *S-N* curve, and the established *S-N* curve with 95% survival probability is slightly higher than the one through regression analysis neglecting run-outs.
4. The fatigue push-out tests resulted to more conservative results compared with the beam test no matter if the stud connectors were placed in orthotropic steel-UHPC composite deck or in traditional steel-NC composite beam. The shear stress redistribution of the stud connectors in the beam test might contribute to the beam results because of the larger number of stud connectors in the shear span compared to the push-out test.
5. The *S-N* curves of stud connectors in current specifications lie below the ones of short-headed stud connectors embedded in UHPC layer no matter obtained from the push-out test or the beam test. And the current specifications make a more conservative arrangement of the short-headed stud connectors in orthotropic steel–UHPC composite bridge deck when used in design.
6. The *S-N* curve with 95% survival probability obtained through the push-out test, and that established through the beam test on the basis of the MLE approach are recommended as a lower bound and an upper bound for the fatigue design of the short-headed stud connectors used in orthotropic steel–UHPC composite bridge deck, respectively.

Declaration of Competing Interest

The authors declare that they have no known competing financial interests or personal relationships that could have appeared to influence the work reported in this paper.

Acknowledgements

The financial support provided by the National Natural Science Foundation of China (Grant NO. 51978501) is greatly appreciated by the authors.

References

[1] Shao X, Yi D, Huang Z, Zhao H, Chen B, Liu M. Basic Performance of the Composite Deck System Composed of Orthotropic Steel Deck and Ultrathin RPC Layer. J Bridg Eng 2013;18(5):417–28.
[2] Benjamin AG. Material Property Characterization of Ultra-High Performance Concrete. Federal Highway Administration 2006.
[3] Buitelaar P, Braam CR, Kaptijn N. Reinforced high performance concrete overlay system for steel bridges. 2004 Orthotropic Bridg Conf 2004.
[4] Walter R, Olesen JF, Stang H, Vejrum T. Analysis of an Orthotropic Deck Stiffened with a Cement-Based Overlay. J Bridg Eng 2007;12(3):350–63.
[5] Dieng L, Marchand P, Gomes F, Tessier C, Toutlemonde F. Use of UHPFRC overlay to reduce stresses in orthotropic steel decks. J Constr Steel Res 2013;89:30–41. https://doi.org/10.1016/j.jcsr.2013.06.006.
[7] Cao J, Shao X, Deng Lu, Gan Y. Static and Fatigue Behavior of Short-Headed Studs Embedded in a Thin Ultrahigh-Performance Concrete Layer. J Bridg Eng 2017;22 (5):04017005. https://doi.org/10.1061/(ASCE)BE.1943-5592.0001031.
[8] Kim JS, Kwark J, Joh C, Yoo SW, Lee KC. Headed stud shear connector for thin ultrahigh-performance concrete bridge deck. J Constr Steel Res 2015;108:23–30. https://doi.org/10.1016/j.jcsr.2015.02.001.
[9] Wang J, Qi J, Tong T, Xu Q, Xiu H. Static behavior of large stud shear connectors in steel-UHPC composite structures. Eng Struct 2019;178:534–42. https://doi.org/10.1016/j.engstruct.2018.07.058.
[10] Tong L, Chen L, Wen M, Xu C. Static behavior of stud shear connectors in high-strength-steel–UHPC composite beams. Eng Struct 2020;218:110827. https://doi.org/10.1016/j.engstruct.2020.110827.
[11] Cao J, Shao X. Finite element analysis of headed studs embedded in thin UHPC. J Constr Steel Res 2019;161:355–68. https://doi.org/10.1016/j.jcsr.2019.03.016.
[12] Z S. Basic performance of a lightweight composite bridge deck with open ribs. Master's Thesis, Hunan University, 2016.
[13] European Committee for Standardization. Eurocode 4: Design of composite steel and concrete structures-Part 2: Composite bridges. Brussels, Belgium, 2005.
[14] American Association of State Highway and Transportation Officials. AASHTO LRFD bridge design specification (2007). Washington DC, USA, 2007.
[15] National Railway Administration of the People's Republic of China. TB 10091-2017. Code for Design on Steel Structure of Railway Bridge. China Railway Publishing House 2017.
[16] King DC, Slutter RG, Driscoll Jr. GC. Fatigue strength of 1/2-inch stud shear connectors 1965:78–106.
[17] Deric B, Oehlers J. Deterioration in strength of stud connectors in composite bridge beams. J Struct Eng 1990;116:3417–31.
[18] Roberts TM, Dogan O. Fatigue of Welded Stud Shear Connectors in Steel-Concrete-Steel Sandwich Beams. J Constr Steel Res 1998;45(3):301–20. https://doi.org/10.1016/S0143-974X(97)00070-9.
[19] Lee P-G, Shim C-S, Chang S-P. Static and fatigue behavior of large stud shear connectors for steel-concrete composite bridges. J Constr Steel Res 2005;61(9): 1270–85. https://doi.org/10.1016/j.jcsr.2005.01.007.
[20] Ovuoba B, Prinz GS. Fatigue Capacity of Headed Shear Studs in Composite Bridge Girders. J Bridg Eng 2016;21(12):04016094. https://doi.org/10.1061/(ASCE)BE.1943-5592.0000915.
[21] Hanswille G, Porsch M, Ustundag C. Resistance of headed studs subjected to fatigue loading. Part I: Experimental study. J Constr Steel Res 2007;63(4):475–84. https://doi.org/10.1016/j.jcsr.2006.06.035.
[22] Roger G. Slutter JWF. Fatigue strength of shear connectors. vol. 315. 1966.
[23] Hobbacher AF. Erratum to: Recommendations for Fatigue Design of Welded Joints and Components. 2019. https://doi.org/10.1007/978-3-319-23757-2_8.
[24] Spindel J, Haibach E. The method of maximum likelihood applied to the statistical analysis of fatigue data. Int J Fatigue 1979;1(2):81–8. https://doi.org/10.1016/0142-1123(79)90012-4.
[25] Pollak RD, Palazotto AN. A comparison of maximum likelihood models for fatigue strength characterization in materials exhibiting a fatigue limit. Probabilistic Eng Mech 2009;24(2):236–41. https://doi.org/10.1016/j.probengmech.2008.06.006.
[26] Strzelecki P. Determination of fatigue life for low probability of failure for different stress levels using 3-parameter Weibull distribution. Int J Fatigue 2021;145: 106080. https://doi.org/10.1016/j.ijfatigue.2020.106080.
[27] Bonaiti L, Gorla C. Estimation of gear SN curve for tooth root bending fatigue by means of maximum likelihood method and statistic of extremes. Int J Fatigue 2021; 153:106451. https://doi.org/10.1016/j.ijfatigue.2021.106451.
[28] MOT (Ministry of Transport of the People's Republic of China). JTG D64-2015. Specifications for Design of Highway Steel Bridge. China Communications Press 2015.
[29] AQSIQ(General Administration of Quality Supervision, Inspection and Quarantine of the People's Republic of China). GB/T 10433-2002. Cheese head studs for arc stud welding. AQSIQ 2002.
[30] MOT (Ministry of Transport of the People's Republic of China). JTG 3362-2018. Specifications for Design of Highway Reinforced Concrete and Prestressed Concrete Bridges and Culverts. China Communications Press 2018.
[31] AQSIQ(General Administration of Quality Supervision, Inspection and Quarantine of the People's Republic of China). GB/T 228-2202. Metallic materials-Tensile testing at ambient temperature. AQSIQ 2002.
[32] MCS-EPFL. Ultra-High Performance Fibre Reinforced Cement-based composites (UHPFRC) Construction material , dimensioning und application. Lausanne, Switzerland, 2016.
[33] CECS(China Association for Engineering Construction Standardization) CECS13: 2009. Standard test methods for fiber reinforced concrete. China Plan Press 2009.

[34] Miner MA. Cumulative Damage in Fatigue. J Appl Mech 1945;12:A159–64. https://doi.org/10.1115/1.4009458.
[35] Yu-Hang W, Jian-Guo N, Jian-Jun L. Study on fatigue property of steel-concrete composite beams and studs. J Constr Steel Res 2014;94:1–10. https://doi.org/10.1016/j.jcsr.2013.11.004.
[36] Xu C, Su Q, Masuya H. Static and fatigue performance of stud shear connector in steel fiber reinforced concrete. Steel Compos Struct 2017;24:467–79. https://doi.org/10.12989/scs.2017.24.4.467.
[37] Zhang Q, Liu Y, Bao Y, Jia D, Bu Y, Li Q. Fatigue performance of orthotropic steel-concrete composite deck with large-size longitudinal U-shaped ribs. Eng Struct 2017;150:864–74. https://doi.org/10.1016/j.engstruct.2017.07.094.
[38] Liu Y, Zhang Q, Meng W, Bao Y, Bu Y. Transverse fatigue behaviour of steel-UHPC composite deck with large-size U-ribs. Eng Struct 2019;180:388–99. https://doi.org/10.1016/j.engstruct.2018.11.057.
[39] Liu Y, Zhang Q, Bao Yi, Bu Y. Fatigue behavior of orthotropic composite deck integrating steel and engineered cementitious composite. Eng Struct 2020;220:111017. https://doi.org/10.1016/j.engstruct.2020.111017.
[40] Liu Y, Zhang Q, Bao Y, Bu Y. Static and fatigue push-out tests of short headed shear studs embedded in Engineered Cementitious Composites (ECC). Eng Struct 2019;182:29–38. https://doi.org/10.1016/j.engstruct.2018.12.068.
[41] Chen S, Huang Y, Gu P, Wang JY. Experimental study on fatigue performance of UHPC-orthotropic steel composite deck. Thin-Walled Struct 2019;142:1–18. https://doi.org/10.1016/j.tws.2019.05.001.
[42] C. Liu, J. Fan, J. N, J. H, J. C LT. Fatigue performance research of headed studs in steel and ultra-high performance concrete composite deck. China J Highw Transp 2017;30:139–46. https://doi.org/10.19721/j.cnki.1001-7372.2017.03.015.
[43] Yuan Y, Wu C, Jiang X. Experimental study on the fatigue behavior of the orthotropic steel deck rehabilitated by UHPC overlay. J Constr Steel Res 2019;157:1–9. https://doi.org/10.1016/j.jcsr.2019.02.010.
[44] Feng Z, Li C, He J, Ke Lu, Lei Z, Vasdravellis G. Static and fatigue test on lightweight UHPC-OSD composite bridge deck system subjected to hogging moment. Eng Struct 2021;241:112459. https://doi.org/10.1016/j.engstruct.2021.112459.
[45] Liu Y. Fatigue failure mechanism of steel-high performance concrete composite bridge deck with large-size u-ribs. Doctoral Thesis, Southwest Jiaotong University, 2019.

Further reading

[6] Unterweger H, Novak F. Strengthening of orthotropic steel decks using UHPC: UHPC-concrete instead of asphalt layer for additional at least 50 years in service. Eurosteel 2017: 8th European Conference on Steel and Composite Structures 2017;1:4502–11. https://doi.org/10.1002/cepa.510.